

Building Service Engineering Research and Technology

<http://bse.sagepub.com>

Transients in natural ventilation A time-periodically-varying source

Diogo Bolster and CP Caulfield

BUILDING SERV ENG RES TECHNOL 2008; 29; 119

DOI: 10.1177/0143624407087849

The online version of this article can be found at:
<http://bse.sagepub.com/cgi/content/abstract/29/2/119>

Published by:

 SAGE Publications

<http://www.sagepublications.com>

On behalf of:



<http://www.cibse.org>
The Chartered Institute of Building Services Engineers

Additional services and information for *Building Service Engineering Research and Technology* can be found at:

Email Alerts: <http://bse.sagepub.com/cgi/alerts>

Subscriptions: <http://bse.sagepub.com/subscriptions>

Reprints: <http://www.sagepub.com/journalsReprints.nav>

Permissions: <http://www.sagepub.com/journalsPermissions.nav>

Transients in natural ventilation – A time-periodically-varying source

Diogo Bolster^a and CP Caulfield^b

^aDepartment of Mechanical and Aerospace Engineering, University of California, San Diego, USA

^bBP Institute & Department of Applied Mathematics and Theoretical Physics, University of Cambridge, UK

We examine the transient behaviour of a naturally ventilated space with a time-varying heat source. The flow is modelled using the ‘emptying filling box’ model developed by Linden et al.¹ with an isolated heat source, modelled as a plume. Scaled laboratory experiments were conducted in a water bath using a brine solution to generate density differences. The room is connected to the exterior via high and low level openings. A natural ventilation flow leads to a two-layer flow with warm fluid in the upper layer and ambient fluid in the lower ‘occupied’ layer. During the flow’s transient evolution, the upper layer has a non-uniform stratification within it, which we study using a simple numerical model. The time-varying stratification leads to time-varying flow rates through the space. We identify four important flow rates and illustrate which of these dominate based on the strength and oscillation period of the thermal source.

Practical applications: Most of the current models for natural ventilation assume a steady state and constant heat loads. Many real heat sources are not constant in time and vary in some quasi-periodic manner. In this work, we show that there are four characteristic flow rates associated with such heat sources. Depending on the strength and period of the source these can vary significantly. In this paper, we show how to calculate these flow rates and select which one should be chosen from a design perspective.

List of symbols

A	Room cross-sectional area	Q_T	Volume flux out of space
A^*	Weighted vent area	a_v	Dimensionless vent area
C	Dimensionless density	a	Dimensionless cross-sectional area
F	Plume buoyancy flux	b	Plume radius
F_I	Increased source buoyancy flux	g	Gravitational acceleration
F_R	Reduced source buoyancy flux	g'	Reduced gravity
\bar{F}	Average source buoyancy flux	f	Dimensionless plume buoyancy flux
H	Height of room	m	Dimensionless plume momentum flux
I	Integral of buoyancy in upper layer	q	Dimensionless plume volume flux
M	Plume momentum flux	\bar{q}	Average of increased and decreased flow rates
Q	Plume volume flux	q_f	Flow rate associated with average source buoyancy flux
Q_B	Volume flux into space	q_I	Flow rate associated with increased source buoyancy flux
		q_R	Flow rate associated with reduced source buoyancy flux

Address for correspondence: Diogo Bolster, Department of Mechanical and Aerospace Engineering, University of California, San Diego, USA. E-mail: dbolster@ucsd.edu

r	Radial coordinate in plume
t	Time
w_a	Vertical velocity in ambient
w_p	Vertical velocity in plume
w^*	Dimensionless vertical velocity in ambient
z	Vertical coordinate
α	Plume entrainment coefficient
ρ	Density
ρ_a	Density in ambient (outside plume)
ρ_{a0}	Density of inflowing ambient fluid
ρ_o	Reference density
τ	Dimensionless time
ζ	Dimensionless vertical coordinate
Γ	Virtual origin parameter for plume
Ω	Frequency at which source conditions change
$\hat{\Omega}$	Dimensionless frequency at which source conditions change

1 Background

Almost one third of the world's energy is used by building services, of which a significant portion is expended on ventilation. A better understanding of ventilation is necessary in order to conceive and operate more efficient ventilation systems. Knowledge of the manner in which air mixes within buildings is key to this understanding since with it better control systems and ventilation schemes can be designed.

In particular, it is important to understand how the thermal stratification in a room develops due to a localised source of heat. Many heat sources, such as people, machinery and computers, can be regarded as localised and understanding the manner in which they stratify a space is critical to design adequate ventilation schemes. These heat sources can often be modelled as an ideal plume, if it is a pure source of buoyancy (e.g. a radiator, a person, a computer). A specific design issue is understanding the flow rates which may be

driven through the space by the buoyancy force, as the flow rate is a key attribute of any natural ventilation strategy, which involves a substantial reduction in energy requirement compared to conventional mechanical ventilation.

2 Review of similar studies

Much work has been done looking at the mixing generated by a buoyant plume within a confined space. The plume is modelled using the classical plume theory developed by Morton et al.² [MTT56]. Baines and Turner³ [BT69] developed a model for the interaction between a buoyant plume and the background environment in a closed room. They considered the flow that develops when an isolated source of buoyancy alone issues into the closed space. This model has come to be known as the 'filling box' model. Asymptotic expressions for the long time density profiles were developed, which were later improved by Worster and Huppert⁴ with an approximate analytic expression. Germeles⁵ developed a reduced numerical method to study the 'filling box' model which allows the inclusion of not just a pure buoyancy source, but also a source of mass and momentum.

In a seminal paper Linden et al.¹ considered the emptying filling box flow, where high and low level openings allow a flow driven by buoyancy differences between the interior and exterior to develop through the box. They showed that a two-layer steady-state stratified system develops in the room with ambient fluid beneath the interface and buoyant fluid above it. They showed, that for an ideal plume source with constant buoyancy flux, the height of the dividing interface depends only on the vent areas and not on the source buoyancy flux. However, it is important to appreciate that both the density of the buoyancy layer, and the flow through the space do vary with the source buoyancy flux.

This variation of flow rate is particularly important to the application of these results to real building ventilation as the flow through the space must be maintained in a range consistent with comfort.

The aforementioned ventilation work looks only at the steady states associated with the flow. Kaye and Hunt⁶ considered the transient response of an emptying filling box, initially filled with ambient exterior fluid when the source buoyancy is started discontinuously. They found that in general the interface ‘overshot’ its final location before relaxing back to its steady state value. Moreover, real sources are likely to exhibit some time dependence in their source conditions, as for example the heat load is likely to change with time. Killworth and Turner⁷ studied the filling box model in a closed box for a pure plume with a time varying buoyancy flux. They noted that if the amplitude of the variation in the source buoyancy flux was sufficiently large, at various times in the cycle the rising plume fluid would actually become dense relative to the fluid in the buoyant layer. This is unsurprising because the less dense fluid in the buoyant layer is associated with source conditions of higher buoyancy flux at different stages in the cycle. They found that, since the plume fluid typically has non-zero momentum at the height of zero buoyancy, it became a fountain and eventually stalled at the level of zero momentum. Additionally they found that modelling the spread of the plume at the level of zero buoyancy better matched experimental data than modelling the plume spread at the level of zero momentum.

In order to understand this spreading of the plume below the top of the room Kumagai⁸ studied the ‘filling box’ model for a room which initially has two distinct density layers in it, a heavy layer on the bottom and light one on top, which permits the plume to impinge on the density interface, spread out, and entrain fluid along the interface.

Cardoso and Woods⁹ built further on this work by looking at a box where there is initially a stable linear density gradient. As in Killworth and Turner⁷ they found that the plume will spread at the zero-buoyancy level and so entrainment occurs along an interface in fashion similar to that found by Kumagai⁸. A long-time model for this entrainment based on energetics was also presented. Bower¹⁰ considered a related flow in the emptying filling box, when the source buoyancy flux is switched from one value to another. He identified two qualitatively different behaviours. When the source buoyancy flux was increased, the plume fluid ‘punched through’ the existing buoyant layer to the ceiling, and the initial buoyancy layer was eroded through entrainment by the rising plume, filling the room from the ceiling. Conversely, when the source buoyancy flux was reduced, analogously to the situation identified by Killworth and Turner⁷, the rising plume was dense compared to the initial buoyant layer, and hence a new layer intruded below the initial layer. Bower found that, provided the amplitude of the variation between buoyancy fluxes was sufficiently large, the rising fluid spread below the previous buoyant layer with little entrainment, and the initial buoyant layer was eroded principally by draining through the upper opening.

3 Introduction

The work presented here is intended to consider the related and important problem of the emptying filling box with a source whose buoyancy flux does not merely switch from one value to another, but pulsates with some frequency. We model situations where the heat load is changing without being controlled (e.g. equipment being turned on and off, people walking in and out of a room, etc.), where the ideal plume analysis is relevant.

The following model considers the case where the initial source buoyancy flux is high. Then for some reason (e.g. machinery being turned on and off, people moving in and out of the space etc.) the source buoyancy flux is reduced. We consider situations where the source buoyancy flux jumps between two values at various frequencies. In our model we look at the case where the natural ventilation interface (determined by the geometry of the room alone) is at about half the height of the room, because this seems most applicable to reality and also allows for the best visualisation. As a control case we consider the situation where the buoyancy flux corresponds to the average of the upper and lower values. We are particularly interested in two aspects of the flow. Firstly, we wish to consider the transient response of the layer depth and flow rates to the variation in the source conditions. Secondly, we wish to identify how much the time-averaged flow rate through the room is affected by varying the source buoyancy flux.

The structure of the paper is as follows: In Section 4 the details of the model are described. In Section 5 the numerical scheme is described and results for various conditions are presented. Section 6 describes analogue experiments, while in Section 7 the experimental measurements are compared to the results of our numerical model. Section 8 discusses the application of the model to a real-life ventilation scenario, and conclusions are drawn in Section 9.

4 Model description

4.1 Plume model

To model our isolated source of buoyancy, we utilise the classical model of MTT56, under the Boussinesq approximation (i.e., we assume that density variations only play a significant role in the buoyancy force). This model is based on evolution equations for the three important bulk properties of

the plume:

$$\begin{aligned} \frac{dQ}{dz} &= 2\alpha M^{1/2}, & M \frac{dM}{dz} &= FQ, \\ \frac{dF}{dz} &= \frac{g}{\rho_0} \frac{d\rho_a}{dz} Q, \end{aligned} \tag{1}$$

where πQ is the volume flux, πM is the momentum flux and πF is the buoyancy flux:

$$\begin{aligned} Q(z) &= 2 \int_0^\infty r w_p dr = \bar{w}_p b^2, \\ M(z) &= 2 \int_0^\infty r w_p^2 dr = \bar{w}_p^2 b^2, \\ F(z) &= 2 \int_0^\infty r w_p g \frac{\rho_a - \rho_p}{\rho_0} dr \\ &= g \frac{\rho_a - \bar{\rho}_p}{\rho_0} \bar{w}_p b^2 = \bar{g}'_p Q \end{aligned} \tag{2}$$

The quantity α is the entrainment constant defined in MTT56, which relates the vertical velocity scale in the plume to the entrainment velocity on the edge of the plume and is a fundamental assumption of the model.

In the above equations, $w_p(r, z)$ and $\rho_p(r, z)$ are the vertical velocity and density profiles in the plume, respectively, ρ_a is the ambient density and ρ_0 is a reference density, averaged over a sufficiently long time scale to capture the mean properties of the inevitable turbulent fluctuations. However, we are interested in the response of the system to a time variation in the source conditions over times longer than these characteristic turbulent time scales. Therefore, in general, the fluxes Q , M and F are functions of both z and t (see Conroy et al.¹¹ for a detailed discussion of the appropriate scalings required for this quasi-steady approximation to be valid). For simplicity top-hat variables, defined to be constant within the plume (with characteristic radius $b(z)$) and zero outside the plume, have been chosen and are indicated with

an overbar. Equivalently the governing equations can be thought of as equations for this averaged plume radius, $b(z, t)$, velocity $w(z, t)$ and reduced gravity $g'_p(z)$.

4.1.1 Boundary conditions

The simplest situation is a so called ‘point source’ plume, which is a source of buoyancy where $Q(0, t) = M(0, t) = 0$ and $F(0, t)$ is fixed. (This corresponds to $b(z=0) = 0$, $g'_p \rightarrow -\infty$ and $w_p \rightarrow \infty$). We generalise this to the situation where $F(z=0, t)$ is

$$F(0,t) = \left(\frac{F_I + F_R}{2}\right) + \left(\frac{F_I - F_R}{2}\right) \text{sgn}(\sin(2\pi\Omega t)) \quad (3)$$

i.e. $F(0)$ can take one of two values, F_I or F_R and it jumps between these two values with a frequency Ω . We define the average source buoyancy flux \bar{F} and the ratio of the buoyancy fluxes χ as

$$\bar{F} = \left(\frac{F_I + F_R}{2}\right) \quad \text{and} \quad \chi = \left(\frac{F_I}{F_R}\right) \geq 1. \quad (4)$$

To close the system, the vertical ambient density profile needs to be determined. We consider the flow shown schematically in Figure 1. We are specifically interested in the response of the filling-box flow to this sudden change in conditions, and so we do not consider the subtleties of the plume flows adjustment directly after switching from one source condition to the other (see Scase et al.¹² for a detailed discussion of this situation).

4.1.2 The BT69 filling box model

We follow the approach of Baines and Turner³. We assume that the cross-sectional area A of the room is sufficiently large such that at all heights in the room the plume occupies a negligible fraction of the area, i.e. $b(z) \ll A$ for $0 < z < H$. Therefore, the

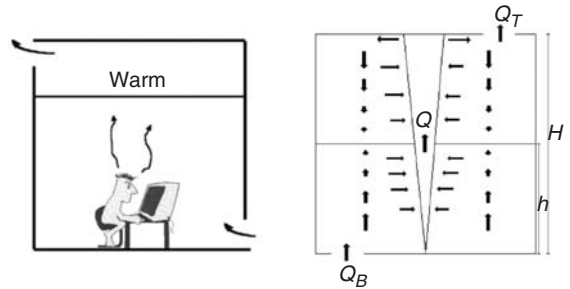


Figure 1 Illustration of a naturally ventilated space. Left figure illustrates thermal plume rising of occupant and equipments. The right figure represents the idealised system

entrainment into the plume is horizontal and the MTT56 plume equations written above can still be applied. When the plume impinges on the ceiling it spreads horizontally like a gravity current. Provided that the aspect ratio of the room is sufficiently small the resulting flow will descend into the box. BT69 shows that as long as the assumption $b \ll A$ holds the return flow can be found using volume conservation:

$$w_a A = -\pi(Q - Q_T) \quad (5)$$

where w_a is the vertical velocity outside the plume and Q_T is the volume flow rate leaving the box through the upper vent. If the flow is of a sufficiently large scale for advection to dominate diffusion, the conservation of mass equation become:

$$\frac{\partial \rho_a}{\partial t} - \pi(Q - Q_T) \frac{\partial \rho_a}{\partial z} = 0 \quad (6)$$

Provided the evolution of the room density occurs on a very much slower time scale than the time required for the plume to rise through the room (i.e. provided the room has a small aspect ratio $((5/6\alpha)^2 (A/\pi H^2)) \gg 1$) we may assume that the plume rises through a quasi-steady ambient density distribution (see BT69 for more discussion). To close our system we need to determine Q_T , the flow rate through the upper vent. Assuming that the source has no volume flux, conservation of volume

implies that $Q_T = -Q_B$ (where we use the convention that negative fluxes correspond to flow into the room). If we assume that the pressure distribution is hydrostatic and that Bernoulli's equation applies it is straightforward to show that:

$$Q_T = Q_B = A_* \sqrt{I_C}, \quad A_* = \frac{A_{\text{top}}^2 A_{\text{bot}}^2}{1/2(A_{\text{top}}^2 + A_{\text{bot}}^2)}$$

and
$$I_C = \int_h^H g' dz \tag{7}$$

where discharge coefficients have been absorbed into the opening areas for clarity. I_C quantifies the effect of the total buoyancy in the room on the hydrostatic pressure, while A_* is the effective opening area. (See Linden et al.¹ and Woods et al.¹³ for a more detailed derivation.) At steady state the buoyant upper layer is well mixed, with $I_C = g'_\infty(H - h)$, where g'_∞ is the reduced gravity of the fluid entering the buoyant layer via the plume.

Using the well-known similarity solution for the volume and momentum fluxes in an unstratified fluid (Morton et al.²)

$$F(z) = F_S, \quad Q(z) = \frac{6\alpha}{6} \left(\frac{9\alpha}{10} F_S \right)^{1/3} z^{5/3} \quad \text{and}$$

$$M(z) = \left(\frac{9\alpha}{10} F_S \right)^{2/3} z^{4/3} \tag{8}$$

we choose to scale our system with the mean source buoyancy flux \bar{F} defined in (4) and the room depth H . Therefore, we define the notional volume and momentum fluxes Q_H and M_H as well as a reduced gravity g'_H

$$Q_H = \frac{6\alpha}{5} \left(\frac{9\alpha}{10} \bar{F} \right)^{1/3} H^{5/3},$$

$$M_H = \left(\frac{9\alpha}{10} \bar{F} \right)^{2/3} H^{4/3} \quad \text{and}$$

$$g'_H = \left(\frac{6\alpha}{5} \left(\frac{9\alpha}{10} \right)^{1/3} H^{5/3} \right)^{-1} \bar{F}^{2/3} \tag{9}$$

As the characteristic time scale, we will choose the filling box time scale T_f defined as

$$T_f = \frac{AH}{\pi Q_H} \tag{10}$$

This is the time scale over which a source would completely fill a room in the absence of ventilation. Using these quantities we then scale our system variables as

$$z = \zeta H, \quad C = \frac{\rho_{a0} - \rho}{\rho_0},$$

$$Q = Q_H q, \quad M = M_H m \tag{11}$$

$$F = \bar{F} f, \quad t = T_f \tau,$$

$$A_v = \frac{\pi Q}{\sqrt{g'_H H}} a_v, \quad w = \frac{H}{T_f} w^* \tag{12}$$

Using the above non-dimensionalisation our plume equations become

$$\frac{dq}{d\zeta} = \frac{5}{3} m^{1/2}, \quad m \frac{dm}{d\zeta} = \frac{4}{3} f q,$$

$$\frac{df}{d\zeta} = \frac{q}{q_S} \frac{dC_a}{d\zeta}, \tag{13}$$

where C_a is the ambient concentration. The boundary conditions are

$$f(0) = 1 + 2 \left(\frac{\chi - 1}{\chi + 1} \right) \text{sgn}(\sin(\hat{\Omega} \tau)),$$

$$\hat{\Omega} = \frac{2\pi\Omega}{T_f} \tag{14}$$

where $\hat{\Omega}$ is the dimensionless source frequency. The evolution equation for the room concentration becomes

$$\frac{\partial C}{\partial \tau} - (q - q_T) \frac{\partial C}{\partial \zeta} = 0, \quad q_T = a_v \sqrt{E},$$

$$E = \int_0^1 C d\zeta \tag{15}$$

5 Numerical Model – Germeles algorithm

We can solve this system of equations using a modification of the method originally developed by Germeles⁵. Although this model is well-known and commonly applied, we will briefly review the algorithm, as the possibility of variation in source buoyancy flux leads to some subtle complications. The numerical method relies on the discretisation of the ambient density into a finite number of layers, n . As mentioned before, it is assumed that the plume evolves far more rapidly than the ambient density field, and so at every time step the plume equations are solved (assuming a steady background density gradient) using a fourth-order Runge–Kutta algorithm. The density layers in the background are then advected downwards with a velocity calculated using the discretised version of (5), i.e.

$$w(i) = \frac{q(i) - q_T}{a(i)} \quad (16)$$

where i represents each different layer ($1 < i < n$). Each layer is then advected downwards as follows

$$y_{\text{new}}(i) = y_{\text{old}}(i) + \Delta\tau w(i) \quad (17)$$

This process captures the entrainment of fluid from each layer by the rising plume. If the plume reaches the ceiling, a new layer is added at the top of the room, with an interface location and concentration

$$y_{\text{new}}(n+1) = 1 - \Delta\tau \frac{q(n) - q_T}{a(n)} \quad (18)$$

$$c_{\text{new}}(n+1) = c_{\text{old}}(n) - q_0 \frac{f(n)}{q(n)} \quad (19)$$

This layer contains the volume of fluid arriving at the ceiling during the timestep which does not flow out through the

upper opening. (A new layer of ambient fluid is also introduced at the bottom of the room with depth $Q_B \Delta\tau$, modelling the inflow of ambient fluid.)

The model is somewhat more complicated when the plume does not remain buoyant as it rises. Although the plume fluid undoubtedly overshoots its level of neutral buoyancy, for simplicity we assume that negligible entrainment occurs during this overshoot, and the plume fluid will intrude at its neutral height (as discussed in more detail in Bower¹⁰ this assumption is valid provided that the difference in buoyancy fluxes is sufficiently large). Therefore, below the level of zero buoyancy, the interfaces have velocities as before

$$w(i) = \frac{-q(i) + q_T}{a(i)} \quad (20)$$

while above the level of zero buoyancy

$$w(i) = \frac{q_T}{a(i)} \quad (21)$$

Since there is no flow of the plume through these layers they simply drain upwards due to the outflow through the upper opening. Rather than introducing a new layer of fluid at the top of the box we introduce a new intruding layer at the neutral buoyancy height.

6 Experiments

Instead of discussing the properties of the solutions to this system of equations in isolation it is more useful to compare the predictions of the model to a sequence of analogue experiments. A schematic of the experimental setup is shown in Figure 2 and discussed further here. We used various brine solutions to model density variations in a plexiglas tank of dimension $30 \times 40 \times 30 \text{ cm}^3$, which was submerged within a larger tank

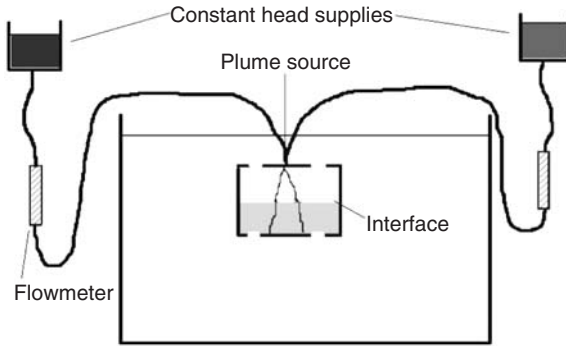


Figure 2 Experimental setup

($2.4 \times 1.2 \times 1.2 \text{ m}^3$) filled with fresh water, representing the external ambient in the model. Several holes were drilled in the top and bottom of the smaller tank to represent the openings in the model. Two plume sources were drilled into the centre of the top of the tank so that at all heights the cross-sectional area of the plume is much less than that of the room. For the sake of ease the source injected negatively buoyant (heavier) fluid from the top of the tank and so represents an inverted form of our model.

The plume source follows a design by Dr Paul Cooper (see Hunt et al.¹⁴ for details) in order to create as close to a turbulent top-hat profile on exit as possible. Due to the small magnitude of the density differences (of the order of a few percent) the so-called Boussinesq approximation is valid, and so the inversion of the flow geometry has no dynamical significance, as density variations only affect the buoyancy force, and have no inertial effect.

Two supply tanks, each with fluid of different density fed one of the plume sources. We could therefore switch easily between the two supplies thus generating a step up or down in source buoyancy. For each experiment red food dye was added to a batch of brine. From this batch the two dense fluid supplies were made. Therefore the fluid injected into the smaller tank has the same relative

dilution of food dye corresponding to the same fluid density, irrespective of which source supplies it. From one side of the large tank we lit the apparatus uniformly while recording from the other side using a digital monochrome CCD camera. We then measure the light intensity of the recorded images using the image analysis software, DigImage (Cenedese and Dalziel¹⁵). This light intensity can then be correlated to the density of the fluid. This is done by periodically drawing a variety of samples from the tank and measuring their density and the associated light intensity.

As discussed in the introduction, in the experiments it is necessary to inject a finite volume flux through the source. It is straightforward to modify the simple model presented above to allow for this using the concept of effective or virtual origin (see Caulfield¹⁶ and Hunt and Kaye¹⁷ for details). As shown in Woods et al.¹³ the height of the interface depends strongly only on the value of the virtual origin. In order to have the same natural ventilation interface associated with both the supplies of salt water we ensure that they have the same virtual origin by forcing the parameter Γ , originally defined by Morton¹⁸, to have the same value for both sources, where

$$\Gamma = \frac{5\sqrt{\pi} Q_0^2 B_0}{4\alpha M_0^{5/2}} \quad (22)$$

Our plume source has a fixed radius b_s and the source momentum flux is assumed to be proportional to Q_0^2/b_s^2 . Therefore, for a given ratio of buoyancy fluxes, two plumes have the same virtual origin, and thus the same steady state interface height, if

$$\frac{g'_l}{g'_u} = \chi^{2/3} \quad \text{and} \quad \frac{Q_l}{Q_u} = \chi^{1/3} \quad (23)$$

We conducted 12 experiments, with three different periods (labelled 'L', 'M' and 'S' for

Table 1 Periods of oscillation and values of χ for the 12 experiments conducted in this study

Experiment number	χ	Length of period	$\hat{\Omega}$
L30	30	$5T_f$	0.2
M30	30	$0.9T_f$	1.11
S30	30	$0.45T_f$	2.22
L10	10	$5T_f$	0.2
M10	10	$0.9T_f$	1.11
S10	10	$0.45T_f$	2.22
L5	5	$5T_f$	0.2
M5	5	$0.9T_f$	1.11
S5	5	$0.45T_f$	2.22
L2	2	$5T_f$	0.2
M2	2	$0.9T_f$	1.11
S2	2	$0.45T_f$	2.22

‘long’, ‘medium’ and ‘short’ period, respectively) and four different values of χ listed in Table 1. In each case it was apparent that the matching process described in (23) worked well and led to close agreement in steady-state interface locations. These experiments span a broad range of the relevant parameter ranges, and so it is natural to discuss the properties of our model system in terms of these parameters, simultaneously illustrating how accurately the model fits the experimental data.

7 Results

In Figures 3 and 4, we show the time varying ambient concentration profiles from experiment L30 from the heating (increased source buoyancy flux) and cooling (reduced source buoyancy flux) stages, respectively. They are shown here to illustrate the three-layer structure that develops during the transient evolution of the flow. We have an upper highly buoyant layer associated with the increased source buoyancy flux, a middle layer of intermediate density associated with the reduced source buoyancy flux and a lower layer of ambient density. It is clear that the numerical model captures the essential features of the flow well. The interfaces between the various

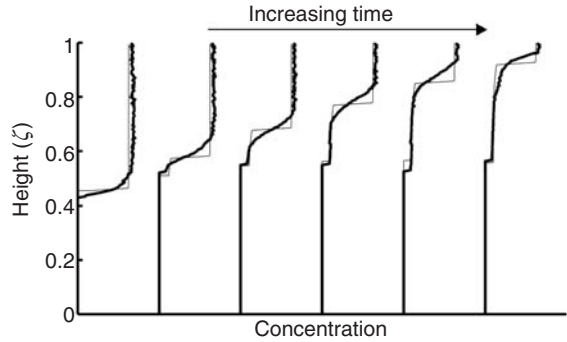


Figure 3 Density profiles during the reducing buoyancy flux stage in experiment L30. The thick line corresponds to the experimental data. The lighter line corresponds to the model

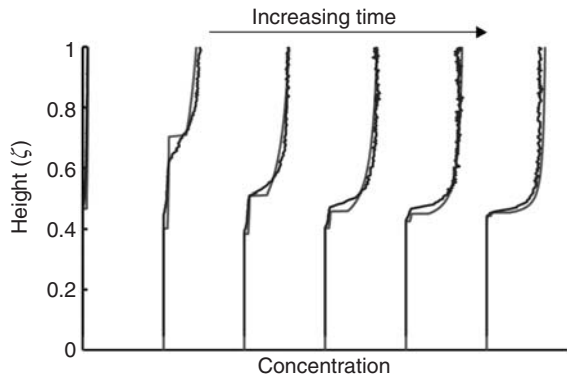


Figure 4 Density profiles in the increasing buoyancy flux stage in experiment L30. The thick line corresponds to the experimental data. The lighter line corresponds to the model

layers change significantly with time, and so in Figures 5–8 we plot as a function of time the location of the two dominant interfaces, h_R and h_I (i.e. the heights defining the lower limits of the buoyant layers associated with the reduced buoyancy flux source (plotted with a thick line) and the increased buoyancy flux (plotted with a thin line). Overall we observe a good agreement between model and our theory.

We first need to consider the validity of our intrusion assumption. We assume that the plume will spread instantaneously at the level

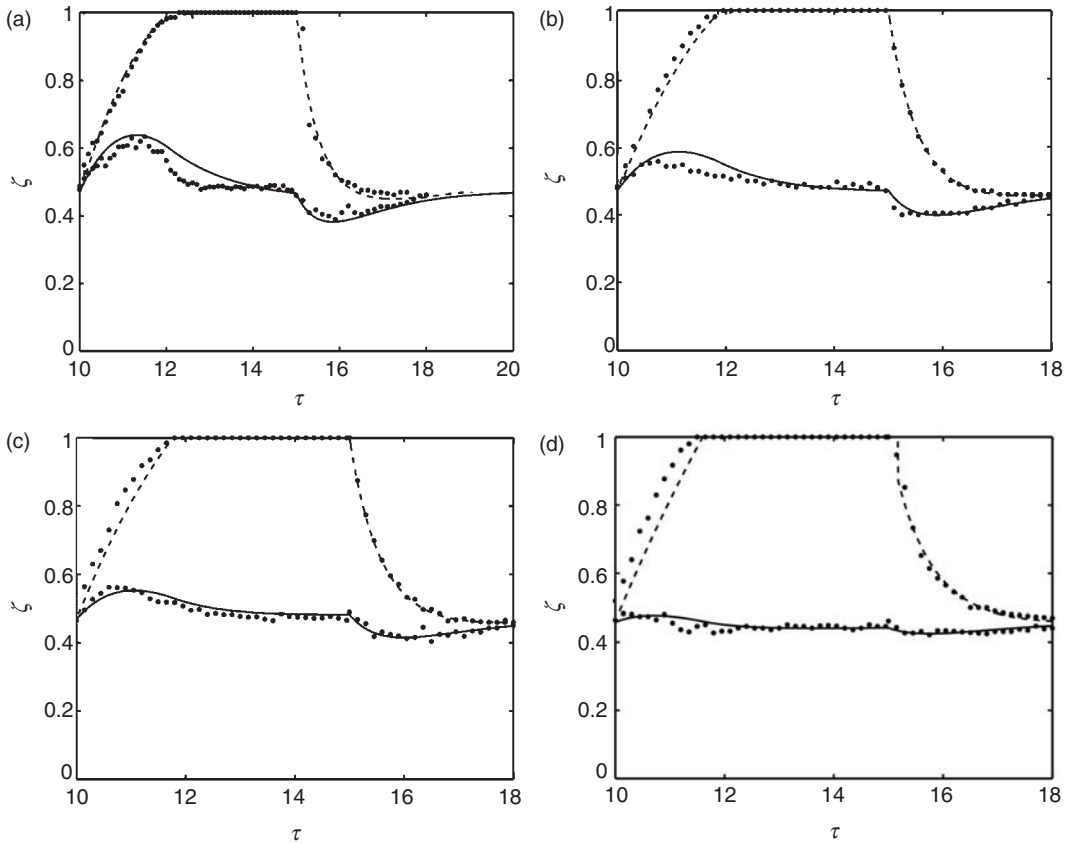


Figure 5 Interface heights for the L experiments, where the forcing period is $57\tau_f$. h_R is plotted with a solid line (-). h_I is plotted with a dashed line (- -). Experimental results are represented by dots (·). (a) $\chi=30$, (b) $\chi=10$, (c) $\chi=5$ and (d) $\chi=2$

of zero buoyancy and that no penetration through this layer takes place. This should affect the location of the upper interface in our experiments. Looking at the results in Figures 5–8, we see that we get very good agreement between theory and experiment when our parameter χ is sufficiently large (i.e. $\chi > 10$). This is unsurprising because a larger value of χ means a larger difference in source buoyancy fluxes. The larger the difference the harder it should be for the reduced buoyancy flux plume to penetrate into the upper layer, which is of course associated with the increased buoyancy flux plume. However, while there is definitely some erosion into the

upper layer for the experiments with smaller values of χ (i.e. 5 and 2) it should be noted that the error is not huge (on the order of 10–15%) and that the qualitative description is good. We also considered the behaviour of a more complicated model (based on the Bloomfield and Kerr¹⁹ model) that captured the fountain dynamics above the level of zero buoyancy. This involves solving six more equations, and we found that the predicted improvements are not sufficiently large to justify the extra computational effort.

Certain characteristics of the flow captured both experimentally and numerically, are worthy of note. When T_f is large (as shown

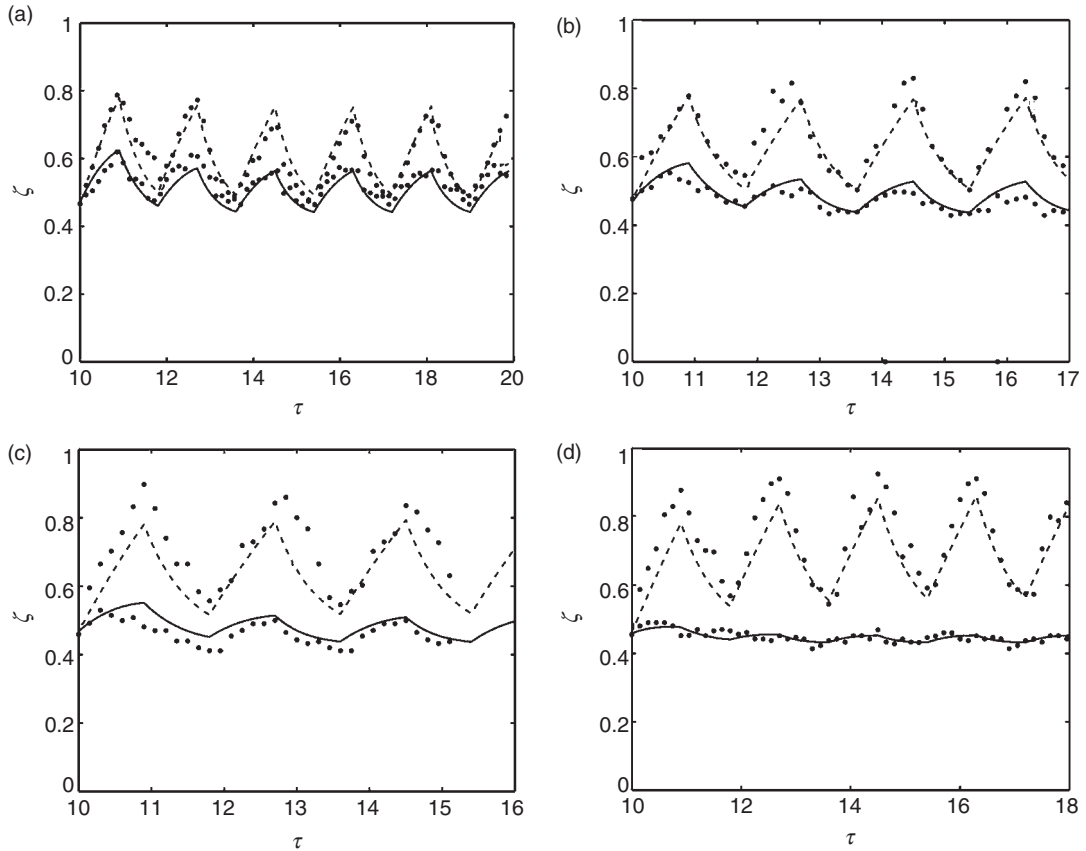


Figure 6 Interface heights for the M experiments, where the forcing period is $0.9T_f$. h_R is plotted with a solid line (-). h_i is plotted with a dashed line (- -). Experimental results are represented by dots (·). (a) $\chi=30$, (b) $\chi=10$, (c) $\chi=5$ and (d) $\chi=2$

in Figure 5) the flow essentially approaches close to steady state for both the increased and reduced source buoyancy fluxes. Moreover, in each case, the transient approach to this steady state is strongly affected by the presence in the chamber of a buoyant layer associated with the previous source buoyancy flux. Initially, since the source buoyancy flux is reduced, the new buoyancy layer intrudes underneath the old (more) buoyant layer, which drains through the upper opening. Since the plume arriving at the interface has a reduced buoyancy flux, it also has a substantially reduced volume flux than before as can be seen from the similarity

solution due to Morton et al.² given in (8) ($Q \propto F^{1/3}$). Therefore, the outflow through the upper opening (essentially driven by the hydrostatic pressure difference associated with the initial buoyant layer) is larger than the arriving plume volume flux and so the total depth of the buoyancy layers decreases initially (see Bower¹⁰ for a detailed discussion of this). As is apparent in Figure 5(a) this transient excursion can be quite substantial when χ is small and hence the source buoyancy flux is substantially reduced. Then the upper buoyant layer typically drains away over approximately two filling box times for the particular interface location

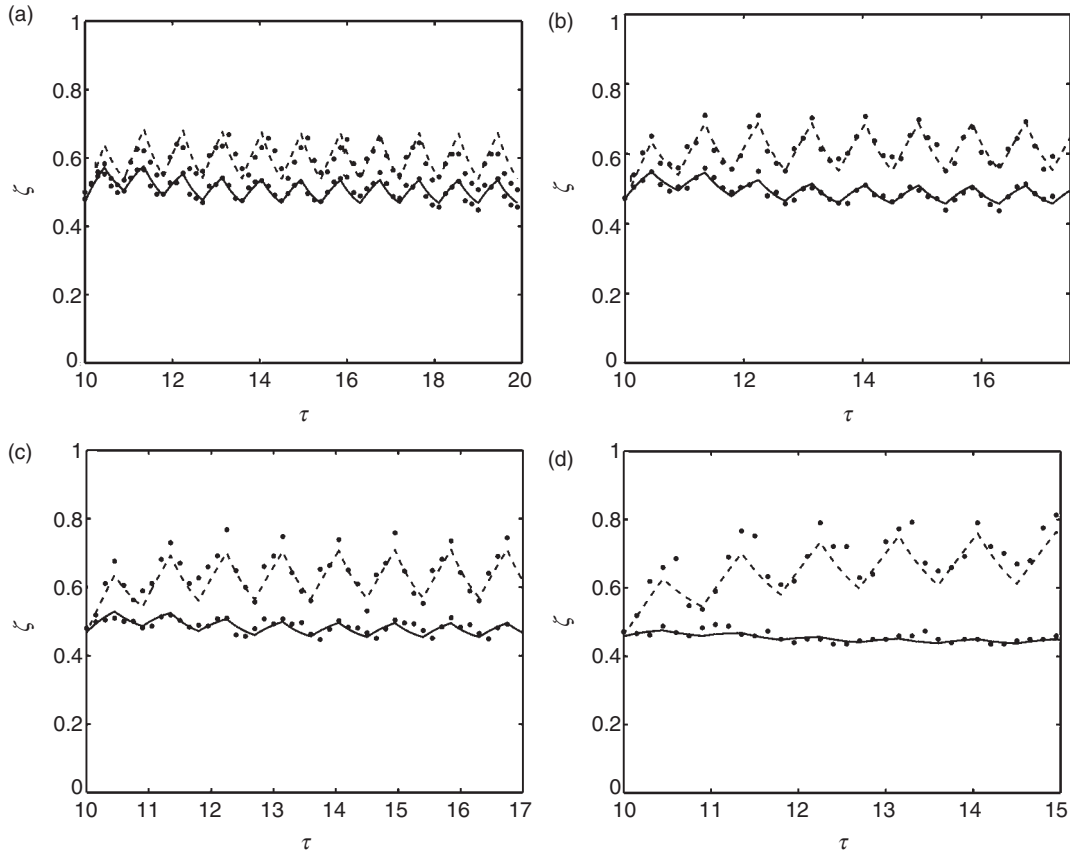


Figure 7 Interface heights for the S Experiments, where the forcing period is $0.457\tau_f$. h_R is plotted with a solid line (-). h_I is plotted with a dashed line (- -). Experimental results are represented by dots (-). (a) $\chi = 30$, (b) $\chi = 10$, (c) $\chi = 5$ and (d) $\chi = 2$

($\zeta = 0.5$) we have chosen. This is consistent with the time scale analysis of Kaye and Hunt⁶ as this is the natural draining time for such a layer.

Subsequently, when the source buoyancy flux reverts to its larger value, the converse happens. The plume ‘punches through’ to the ceiling, and the old layer is eroded through entrainment. Also, the volume flux of the plume arriving at the lower interface has now increased to a value larger than before, which was in balance with the outflow through the upper opening. Therefore, the total depth of the buoyant layers increases, analogously to the transient overshoot observed by Kaye and

Hunt⁶ and Bower¹⁰. This over-shoot is clearly observable, although it is typically smaller in amplitude than the reduction in depth observed when the source buoyancy flux is reduced. Nevertheless, it is apparent that in this stage of the cycle, the intermediate layer is also eroded (this time by entrainment by the more buoyant plume as it punches through and fills the room from the top) over a time scale of approximately two filling box times.

For smaller periods of variation in the source buoyancy flux (as shown in Figure 6 and 7) the upper layer associated with the plume fluid with increased source

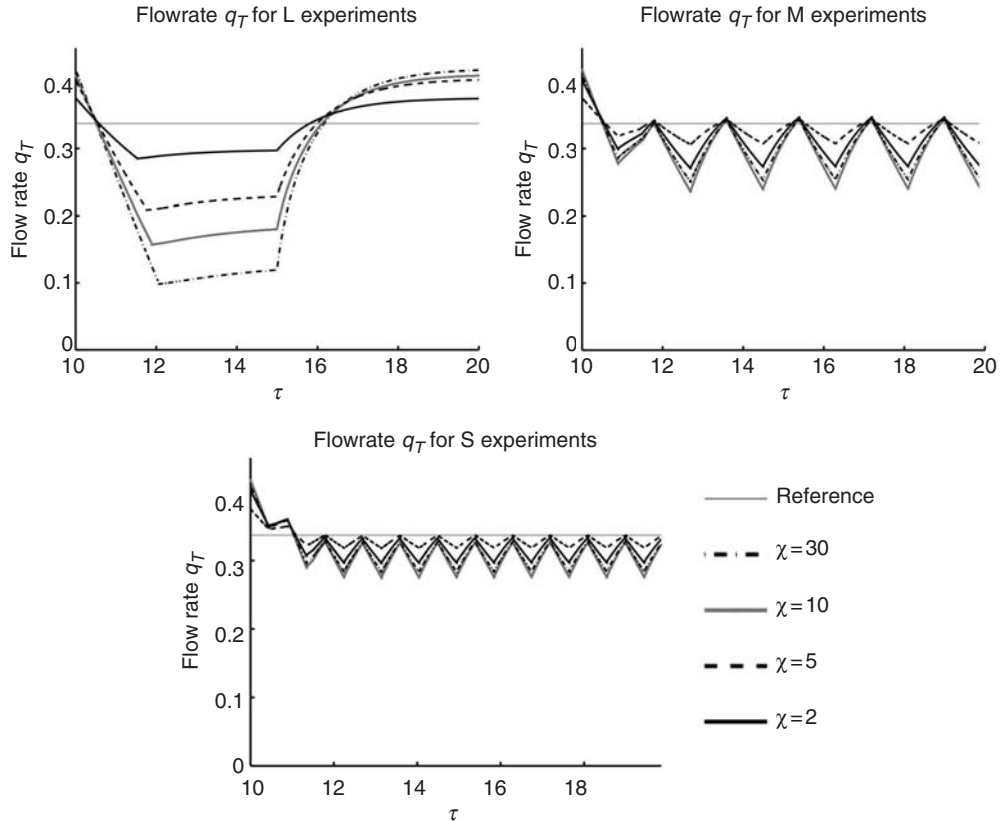


Figure 8 Numerically predicted flow rates through the room for the L, M and S experiments

buoyancy flux, never completely drains away, but there is still a clear oscillation in the location of the interfaces, whose amplitude naturally decreases as $\chi \rightarrow 1$. All these aspects are well captured by the experimental data. The combined effect of the oscillations and the presence of the intermediate layer means that the reduced gravity of the upper layer inevitably changes from its initial value as the plume fluid associated with the increased source of buoyancy flux entrains fluid from the intermediate layer and travels varying distances before arrival in the upper layer. This variation in the density distribution and depth of the upper layer causes a slow adjustment in the mean depth of the upper

layer (most apparent in flows where χ is close to 1, i.e. Figure 7(d), when such small variations are still significant). Nevertheless, in general the flows always eventually evolve into a regime where two buoyant layers oscillate around a constant mean value.

Of course of most interest to flow ventilation is the extent to which oscillation in the source conditions affects the ventilation flow through the chamber. In Figure 8(a)–(c) we plot the numerically calculated flow rates of the various choices of parameters shown in Table 1. Each panel is for a different value of T_f as this proves to be the most natural way to group the results. There are four important steady state flow rates that

should be compared with these calculations namely

$$\begin{aligned}
 q_{\bar{f}} &= \bar{f}^{1/3} \zeta^{5/3}, & q_I &= f_I^{1/3} \zeta^{5/3}, \\
 q_R &= f_R^{1/3} \zeta^{5/3}, & \bar{q} &= \frac{1}{2}(q_I + q_R) \quad (24)
 \end{aligned}$$

In these expressions, $q_{\bar{f}}$ is the steady state flow rate associated with the average of the upper and lower buoyancy fluxes, q_I is the steady state flow rate associated with the increased buoyancy flux, q_R is the steady state flow rate associated with the reduced buoyancy flux and \bar{q} is the average of the upper and lower flow rates, while ζ is the steady state interface location.

We expect the actual flow rate always to lie in the range $q_R < q_T < q_I$. Furthermore, over sufficiently long time intervals, the heat load of the actual sources corresponds to the load associated with a source with mean buoyancy flux \bar{f} , and so the associated volume flow rate $q_{\bar{f}}$ is the most natural control value. Scaling the other flow rates with $q_{\bar{f}}$ (essentially removing the dependence on the depth of the buoyancy layers) we obtain

$$\begin{aligned}
 \frac{q_R}{q_{\bar{f}}} &= \frac{2^{1/3}}{(1 + \chi)^{1/3}}, & \frac{q_I}{q_{\bar{f}}} &= \frac{(2\chi)^{1/3}}{(1 + \chi)^{1/3}}, \\
 \frac{\bar{q}}{q_{\bar{f}}} &= \frac{1 + \chi^{1/3}}{2^{2/3}(1 + \chi)^{1/3}} \quad (25)
 \end{aligned}$$

From these expressions, we can show straightforwardly that $q_R < \bar{q} < q_{\bar{f}} < q_I$. From Figure 8(a)–(d), it is apparent that, unsurprisingly, the flow rate q_T varies with the period of the oscillation of the source conditions, and the amplitude of this variation decreases as $\chi \rightarrow 1$. In all cases the flow rate is less than $q_{\bar{f}}$, although the mismatch decreases as the frequency of variation increases.

For smaller frequency (i.e. Figure 8(a)) the mean flow rate over a whole cycle is closer to \bar{q} , as the flow spends significant periods in each state. However, this agreement is not exact, due to the clear asymmetry between situations

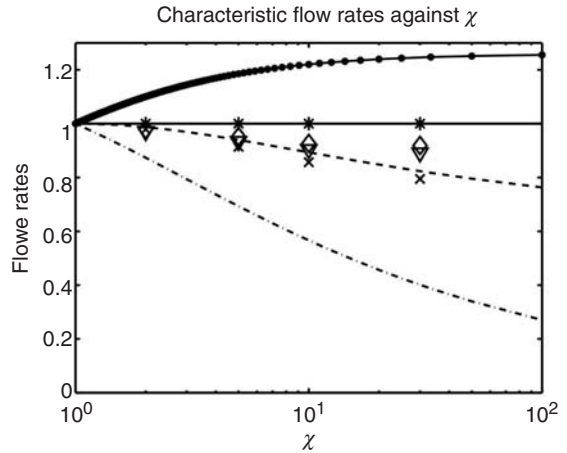


Figure 9 Plot of the four characteristic normalized flow rates for various values of: $q_{\bar{f}}$ (-); q_I (•); \bar{q} (- -); and q_R (- · -). Also shown are the average flow rates from experiments: * marks the ‘reference case’ with mean buoyancy flux; x = L; ∇ = M; ◇ = S

when the buoyancy flux is respectively reduced and increased. When the buoyancy flux is reduced, the flow drops rapidly (due primarily to the simple draining of the upper layer) whereas when the buoyancy flux is increased, due to the inevitable entrainment of the intermediate layer fluid by the more buoyant plume as it ‘punches through’, the flow rate adjusts more slowly and smoothly to higher values.

In Figure 9, we illustrate the effect of this asymmetry by plotting the mean flow rates for each of the experiments as a function of χ against the various average flow rates. It is clear that in general the flow rates lie between \bar{q} and $q_{\bar{f}}$, although for the experiments with $T_f = 5$, the mean flow rate can be slightly less than \bar{q} . However, as T_f decreases $q_T \rightarrow q_{\bar{f}}$ from below as expected and in all cases both q_I and q_R are poor estimators of the actual average flow rate through the room.

8 Discussion and application

It is obviously important to understand how this analysis relates to real applications, and

in particular the characteristic values of the various parameters for real buildings. First let us consider the parameter χ . When $\chi = 1$ this corresponds to the situation where there are no changes in buoyancy (i.e. when a room has reached steady state), which simply recovers the Linden et al.¹ solution and corresponds to a room which has been occupied for a sufficiently long time with no changes in any of the heat sources in a room. When $\chi \rightarrow \infty$ we have a scenario where a heat source is continuously being turned on and off. Large values of χ could correspond to a lecture hall which groups of people enter and exit at regular intervals or a metropolitan train station, which doesn't have a continuous, but rather a discrete and at least quasi-periodic, flux of people through it. Intermediate values of χ would represent an office space where people are regularly entering or leaving and computers or other pieces of equipment are continuously being turned on and off.

In order to find where on Figure 9(a) specific space lies one must determine the appropriate filling box time scale, defined by (10). For example if we consider an office space of cross-sectional area 300 m^2 and height 3 m with a maximum of 100 and average of 85 heat sources (people and equipment moving in and out each contributing 100 W or $0.0028 \text{ m}^4 \text{ s}^{-1}$ to the source buoyancy flux) we get $T'_f \approx 23 \text{ min}$ and $\chi = 1.4$. For this particular case we can see from Figure 9 that there is no significant variation in the average flow rate through the space for high or low frequency changes in source buoyancy flux and so it is not a concern.

However, if we consider a similarly sized space that has a larger variation in source buoyancy, such as a metropolitan transit station where people enter, wait for a train to arrive and leave at essentially periodic intervals, we can have much larger values of χ . If we assume a similar maximum occupancy as the office, \bar{F}_0 will also be smaller. Therefore T_f will be larger, although due to

the dependence of the volume flux on the one-third power of the buoyancy flux, probably not hugely so. For example, if we take maximum occupancy at 100 people and minimum occupancy at 5 people we have $\chi = 20$ and $T'_f \approx 27 \text{ min}$. Now if we look at Figure 9 we see that we can have a variation of up to 20% depending on the frequency at which people enter and leave, which will depend on the frequency of trains.

For example, during rush hour times, trains can arrive and leave in opposite directions as frequently as every 2 min, which corresponds to a characteristic change time of approximately $T_f/30$. At other, quieter times this system can have a much lower arrival and departure frequency, closer to the filling box time. At the quieter times the appropriate average flow rate through the system should be \bar{q} . However, during the rush hour times it is not immediately obvious what the average flow rate through the system will be. It will lie somewhere between \bar{q} and $q_{\bar{f}}$, approaching $q_{\bar{f}}$ asymptotically as the forcing frequency is increased.

Other examples of spaces that would take on large values of χ include theatres, cinemas, classrooms and lecture halls, where large numbers of people enter and exit the given space periodically. In all of these cases though the period of occupancy is several times larger than the filling time scale. Therefore, the most appropriate flow rate to assume would be $q_{\bar{f}}$. Spaces such as corridors and hall ways can have high values of χ and small occupancy times and flow rates closer to $q_{\bar{f}}$ may be appropriate. From Figure 9 it should be evident that \bar{q} is always less than $q_{\bar{f}}$. Therefore, \bar{q} can be thought of as a worst case scenario and as long as it satisfies any minimum air supply standards, these minimum standards will always be met, regardless of the period that the system is being forced at. From a conservative perspective this is the flow rate that should be assumed by design engineers.

For those interested in using these models it is important to highlight some of the assumptions made, which should be considered before applying the results. First, the heat loads considered here are for convective heating only and radiative effects are neglected. Additionally, the experiments and results presented in this paper are for a single heat source well removed from the walls. In practice, multiple plumes that can merge and interact with walls can exist. However, there is no reason why the work presented here could not readily be extended to incorporate such phenomena, should it be required.

9 Conclusions

We have presented a numerical model, based on the Germeles algorithm, to study the transient response of a naturally ventilated space with a periodically time varying heat source. Two dimensionless parameters govern the behaviour of the system. These are $\chi = F_I/F_R$, the ratio of the increased to the reduced source buoyancy fluxes defined in (4), and $\hat{\Omega}$, the dimensionless forcing frequency of the source defined by (14). The dynamics associated with changes in source buoyancy are as follows. When the heat load in a naturally ventilated space is increased, the plume associated with that heat source will ‘punch’ all the way through to the top of the room and spread at the ceiling, filling the upper part of the room from the top. The previous stratification in the upper layer is eroded away by entrainment into the plume. Conversely, when the heat load is decreased, the plume will rise to its level of zero buoyancy where it is decelerated. It will spread at this level, draining the most buoyant fluid above it out of the room. When the change in source buoyancy flux is small the plume may have enough momentum to penetrate into the more buoyant fluid and some erosion of this upper layer will occur by entrainment.

However, for many cases, especially large decreases in source buoyancy flux, this entrainment is negligible and the dynamics are appropriately captured by neglecting it.

A series of small scale laboratory experiments was conducted in order to validate the model. We found that the agreement is very good, particularly when the change in source buoyancy flux is very large (i.e. χ large). Based on observations from our numerical and laboratory experiments we identified two characteristic average flow rates associated with the flow, which based on a real spaces values of the dimensionless parameters χ and $\hat{\Omega}$ can be used to estimate the average flow rate through that space.

For small changes in source buoyancy flux (i.e. χ close to 1) the average flow rate through the system does not vary much regardless of the frequency with which the forcing varies. However, for large changes in source buoyancy flux differences of around 20% (for $\chi = 20$) or larger can exist depending on the frequency of forcing. The higher the forcing frequency is, the larger the average flow rate. In the infinite frequency limit the system approaches a flow rate corresponding to a steady source with a source buoyancy flux equal to the average of the increased and reduced buoyancy fluxes. The variation in average flow rates stems from the nonlinear relationship of the plume volume flow rate with source buoyancy flux (i.e. $Q \propto F^{1/3}$). Therefore, in spaces where large variations in thermal loading occur, it is important to consider the frequency of this forcing in order to estimate an accurate average flow rate through the space.

Acknowledgements

Financial support from the Energy Science and Technology (EST) Program of the University of California Energy Institute (UCEI) and from a Jacobs Fellowship of the Irwin and Joan Jacobs

School of Engineering at the University of California, San Diego are gratefully acknowledged.

References

- 1 Linden PF, Lane-Serff GF, Smeed DA. Emptying Filling Boxes: the Fluid Mechanics of Natural Ventilation. *J Fluid Mech* 1990; 212: 309–35.
- 2 Morton BR, Taylor GI, Turner JS. Turbulent Gravitational Convection from Maintained and Instantaneous Sources. *Proc Roy Soc A* 1956; 234: 1–23.
- 3 Baines WD, Turner JS. Turbulent Buoyant Convection From a Source in a Confined Region. *J Fluid Mech* 1969; 37: 51–80.
- 4 Worster MG, Huppert HE. Time-dependent density profiles in a filling box. *J Fluid Mech* 1983; 132: 457–66.
- 5 Germeles AE. Forced Plumes and Mixing of Liquids in Tanks. *J Fluid Mech* 1975; 71: 601–23.
- 6 Kaye NB, Hunt GR. Time-Dependent Flows in an Emptying Filling Box. *J Fluid Mech* 2004; 520: 135–56.
- 7 Killworth PD, Turner JS. Plumes with Time-varying Buoyancy in a Confined Region. *Geophys Astrophys Fluid Dynamics* 1982; 20: 265–91.
- 8 Kumagai M. Turbulent Buoyant Convection from a Source in a Confined Two-layered Region. *J Fluid Mech* 1984; 147: 105–31.
- 9 Cardoso SSS, Woods AW. Mixing by a Turbulent Plume in a Confined Stratified Region. *J Fluid Mech* 1993; 250: 277–305.
- 10 Bower DJ. Transient Phenomena in Natural Ventilation: Theory and Experiment, 2005. MPhil Thesis, BP Institute, University of Cambridge.
- 11 Conroy DT, Llewellyn Smith SG, Caulfield CP. Evolution of a Chemically Reacting Plume in a Ventilated Room. *J Fluid Mech* 2005; 537: 221–53.
- 12 Scase MM, Caulfield CP, Dalziel SB, Hunt JCR. Time-dependent plumes and jets with decreasing source strengths. *Journal of Fluid Mechanics* 2006; 563: 443–61.
- 13 Woods AW, Caulfield CP, Phillips JC. Blocked Natural Ventilation: the Effect of a Source Mass Flux. *J Fluid Mech* 2003; 495: 119–33.
- 14 Hunt GR, Cooper P, Linden PF. Thermal Stratification Produced by Jets and Plumes in Enclosed Spaces. In Awbi HB ed. *Proc. Roomvent 2000 – 7th International Conference on Air Distribution in Rooms*. New York, Elsevier, 2000: 191–98.
- 15 Cenedese C, Dalziel SB. Concentration and depth fields determined by the light transmitted through a dyed solution. In: *Proceedings of the 8th International Symposium on Flow Visualisation*. 1998: Vol. 8, Paper 061.
- 16 Caulfield CP. Stratification and Buoyancy in Geophysical Flows. 1991; PhD Thesis, DAMTP, Cambridge, University of Cambridge.
- 17 Hunt GR, Kaye NG. Virtual Origin Correction of Lazy Turbulent Plumes. *J Fluid Mech* 2001; 435: 377–96.
- 18 Morton BR. Forced Plumes. *J Fluid Mech A* 1959; 234: 1–23.
- 19 Bloomfield L, Kerr R. A Theoretical Model of a Turbulent Fountain. *J Fluid Mech* 2000; 424: 197–216.